Porous Siloxane Linked Phenylacetylene Nitrile Silver Salts from Solid State Dimerization and Low Polymerization

Y.-H. Kiang, Geoffrey B. Gardner, Stephen Lee,* and Zhengtao Xu

Contribution from the Department of Chemistry and Chemical Biology, Baker Laboratory, Cornell University, Ithaca, New York 14853-1301

Received March 14, 2000

Abstract: Three 3-fold symmetric rigid backbone phenylacetylene nitrile molecules have been prepared to which one to six hydroxy side chains have been attached. These molecules were cocrystallized with silver(I) trifluoromethanesulfonate (triflate) to form microcrystalline porous solids. X-ray powder data show that all three crystal structures are isotypic to the crystal structures found in previous single crystal studies on related systems. Structural models based on these earlier single crystal structures have theoretical powder patterns in reasonable agreement with the experimentally observed patterns. These crystalline materials were allowed to react with silyl triflates. ^{1}H NMR and X-ray powder studies show that the silyl triflate groups react with the alcohol terminated side chains to form siloxane linkages with retention of the initial crystal structure. In the case of 1,3,5-tris(4-((4-cyanophenyl)ethynyl)-2-((4-hydroxybutoxy)methyl)phenylethynyl)benzene, a phenylacetylene nitrile molecule with three alcohol side chains, the introduction of di-*tert*-butylsilyl bis(trifluoromethanesulfonate) resulted in the formation of low polymers with average weight molecular weight of 7×10^4. This polymerized material shows increased chemical robustness in contrast to the unpolymerized material. It is stable in a variety of solvents, including overnight exposure to boiling water. Exchange experiments with toluene show that this final material is still porous.

Introduction

There has been a resurgent interest in extended organic or organometallic crystals based on hydrogen bonds and metal coordination bonds.[1−41] This research has been driven in part by the aesthetic beauty of many of these new systems and in part by the potential use of such materials. Applications explored include catalysis,[42−46] separation,[46−49] magnetism,[50−56] super-

* Author to whom correspondence should be addressed.

(1) Konnert, J.; Britton, D. *Inorg. Chem.* **1966**, *5*, 1193.
(2) Hoskins, B. F.; Robson, R. *J. Am. Chem. Soc.* **1990**, *112*, 1546.
(3) Etter, M. C. *Acc. Chem. Res.* **1990**, *23*, 120.
(4) Abrahams, B. F.; Hoskins, B. F.; Lin, J.; Robson, R. *J. Am. Chem. Soc.* **1991**, *113*, 3045.
(5) Simard, M.; Su, D.; Wuest, J. D. *J. Am. Chem. Soc.* **1991**, *113*, 4696.
(6) Ermer, O.; Lindenberg, L. *Helv. Chim. Acta* **1991**, *74*, 825.
(7) Otieno, T.; Rettig, S. J.; Thompson, R. C.; Trotter, J. **1993**, *32*, 1607.
(8) Michaelides, A.; Kiritsis, V.; Skoulika, S.; Aubry, A. *Angew. Chem., Int. Ed. Engl.* **1993**, *32*, 1495.
(9) Abrahams, B. F.; Hoskins, B. F.; Michail, D. M.; Robson, R. *Nature (London)* **1994**, *369*, 727.
(10) Ung, A.; Gizachew, D.; Bishop, R.; Scudder, M.; Dance, I.; Craig, D. *J. Am. Chem. Soc.* **1995**, *117*, 8475.
(11) Gardner, G. B.; Venkataraman, D.; Moore, J. S.; Lee, S. *Nature (London)* **1995**, *374*, 792.
(12) Lu, J.; Harrison, W. T. A.; Jacobson, A. J. *Angew. Chem., Int. Ed. Engl.* **1995**, *34*, 2557.
(13) Endo, K.; Sawaki, T.; Koyanagi, M.; Kobayashi, K.; Masuda, H.; Aoyama, *Y. J. Am. Chem. Soc.* **1995**, *117*, 8341.
(14) Dolbeq, A.; Boubekeur, K.; Batail, P.; Canadell, E.; Aubansenzier, P.; Coulon, C.; Lerstrup, K. *Mater. Chem.* **1995**, *5*, 1707.
(15) Kuroda-Sowa, T.; Horino, T.; Yamamoto, M.; Ohno, Y.; Maekawa, M.; Munakata, M. *Inorg. Chem.* **1997**, *36*, 6382.
(16) Vaid, T. P.; Lobkovsky, E. B.; Wolczanski, P. T. *J. Am. Chem. Soc.* **1997**, *119*, 8742.
(17) Aakeröy, C. B.; Beatty, A. M.; Leinen, D. S. *J. Am. Chem. Soc.* **1998**, *120*, 7383.
(18) Kobayashi, K.; Koyanagi, M.; Endo, K.; Masuda, H.; Aoyama, Y. *Chem. Eur. J.* **1998**, *4*, 417.
(19) Abrahams, B. F.; Jackson, P. A.; Robson, R. *Angew. Chem., Int. Ed. Engl.* **1998**, *37*, 2656.
(20) Batten, S. R.; Robson, R. *Angew. Chem., Int. Ed. Engl.* **1998**, *37*, 1461.
(21) Kumar, R. K.; Balasubramanian, S.; Goldberg, I. *Inorg. Chem.* **1998**, *37*, 541.
(22) Fujita, M.; Aoyagi, M.; Ogura, K. *Bull. Chem. Soc. Jpn.* **1998**, *71*, 1799.
(23) Li, H.; Eddaoudi, M.; Laine, A.; O'Keeffe, M.; Yaghi, 0. M. *J. Am. Chem. Soc.* **1999**, *121*, 6096.
(24) Li, H.; Eddaoudi, M.; O'Keeffe, M.; Yaghi, O. M. *Nature (London)* **1999**, *402*, 276.
(25) Li, H.; Laine, A.; O'Keeffe, M.; Yaghi, O. M. *Science* **1999**, *283*, 1145.
(26) Kiang, Y.-H.; Gardner, G. B.; Lee, S.; Xu, Z.; Lobkovsky, E. *J. Am. Chem. Soc.* **1999**, *121*, 8204.
(27) Kitazawa, T. *Chem. Commun.* **1999**, 891.
(28) Munakata, M.; Wu, L. P.; Ning, G. L.; Kuroda-Sowa, T.; Maekawa, M.; Suenaga, Y.; Maeno, *N. J. Am. Chem. Soc.* **1999**, *121*, 4968.
(29) Stocker, F. B.; Staeva, T. P.; Rienstra, C. M.; Britton, D. *Inorg. Chem.* **1999**, *38*, 984.
(30) Klok, H. A.; Jollife, K. A.; Schauer, C. L.; Prins, L. J.; Spatz, J. P.; Mö11er, M.; Timmerman, P.; Reinhoudt, D. N. *J. Am. Chem. Soc.* **1999**, *121*, 7154.
(31) Evans, C. C.; Sukarto, L.; Ward, M. D. *J. Am. Chem. Soc.* **1999**, *121*, 1, 320.
(32) Vaid, T. P.; Tanski, J. M.; Pette, J. M.; Lobkovsky, E. B.; Wolczanski, P. T. *Inorg. Chem.* **1999**, *38*, 3394.
(33) Kondo, M.; Okubo, T.; Asami, A.; Noro, S.; Yoshitomi, T.; Kitagawa, S.; Ishii, T.; Matsuzaka, H.; Seki, K. *Angew. Chem., Int. Ed. Engl.* **1999**, *38*, 140.
(34) Bock, H.; Lehn, J. M.; Pauls, J.; Holl, S.; Krenzel, V. *Angew. Chem., Int. Ed. Engl.* **1999**, *38*, 952.
(35) Biradha, K.; Domasevitch, K. V.; Moulton, B.; Seward, C.; Zaworotko, M. J. *Chem. Commun.* **1999**, 1327.
(36) Carlucci, L.; Ciani, G.; Proserpio, D. M. *Angew. Chem., Int. Ed. Engl.* **1999**, *38*, 3488.
(37) Carlucci, L.; Ciani, G.; Proserpio, D. M. *Chem. Commun.* **1999**, 449.
(38) Bontchev, R. P.; Do, J.; Jacobson, A. J. *Inorg. Chem.* **1999**, *38*, 2231.
(39) Lin, K. J. *Angew. Chem., Int. Ed. Engl.* **1999**, *38*, 2730.
(40) Chestnut, D. J.; Kusnetzow, A.; Birge, R. R.; Zubieta, J. *Inorg. Chem.* **1999**, *38*, 2663.
(41) Hagrman, P. J.; Zubieta, J. *Inorg. Chem.* **1999**, *38*, 4480.

10.1021/ja0009119 CCC: $19.00
Published on Web 07/06/2000

conductivity,[57−60] and other electronic properties.[61−65] Despite the scope of the advances, critical problems remain. Chief among them is the inherent stability of the organic or organometallic network. All too often the condition of crystal growth, which in general requires reversible intermolecular bond formation during crystallization, leads to the use of rather fragile coordination or hydrogen bonds to link the organic molecular constituents.[66] It is these same weak intermolecular bonds which are responsible for the poor chemical and thermal stability of the resultant materials.

One approach has been to replace such weak intermolecular bonds by more robust ones such as Ti−O, V−O, Zn−O, and Al−O linkages. The Cambridge Structural Database (CSD) reports respectively 4, 7, 23, and 6 single-crystal structures where organic molecules are joined together into extended networks through these metal−oxygen bonds. Using such bonding, Wolzcanski, Yaghi, and co-workers have recently reported remarkable and promising thermally stable porous solids.[16−24]

At the same time, an examination of the CSD shows that it is extremely difficult to construct crystalline extended solids where the organic molecules are linked to one another through main group bonds such as Si−O, P−O, or S−O close contacts. There is only one report in the CSD of such an Si−O bonded framework[67] and none for either P−O or S−O joined moieties. Existing extended solids of organic molecules held together by O−Si−O bonds involve instead the covalent grafting of organic molecules to preformed silicate and aluminosilicate networks or through the inclusion of an organic component in mesoporous silicate synthesis.[68−74] This absence of atomic length scale crystalline examples in which both organic bonds and Si−O, P−O, or S−O bonds lie in the backbone of the extended framework is all the more noteworthy when one recalls the dominant role that the latter bonds play in the inorganic, biological, and macromolecular literature.

In this paper we report a synthetic methodology for microcrystalline solids in which the organic molecules are bonded to one another through single O−Si−O linkages. This methodology has two parts. In the first step we use fairly weak Ag−N coordination bonds to link 3-fold symmetric rigid phenylacetylene nitrile molecules into a porous honeycomb structure. These phenylacetylene nitrile molecules additionally have covalently attached alkoxymethyl side chains which terminate in hydroxy groups (see Figure 1). In the second step we introduce into these solids reactive silyl triflate ($SiR_n(SO_3CF_3)_m$) guest molecules. The alcohol functionality is nucleophilic and the triflate ion a good leaving group, the result is the displacement of the silyl triflate bond by an Si−O bond involving guest and host. For $SiR_2(SO_3CF_3)_2$ with two triflate leaving groups, this leads to covalent O−Si−O bonds between adjacent phenylacetylene molecules. We find that these reactions occur with retention of the original crystal structure as demonstrated by X-ray powder data. In the case of 1,3,5-tris(4-((4-cyanophenyl)ethynyl)-2-((4-hydroxybutoxy)methyl)phenylethynyl)benzene, a phenylacetylene molecule with three alcohol side chains, the introduction of di-*tert*-butylsilyl bis(trifluoromethanesulfonate) results in the formation of oligomers and low weight polymers with molecular weights up to 10^5.

Experimental Section

General Procedure. Unless otherwise indicated, all commercially available reagents were purchased from Aldrich and used without further purification. Analytical grade solvents were obtained from commercial suppliers (Aldrich, Burdick and Jackson, Fisher Scientific and Mallinckrodt). Anhydrous benzene and acetonitrile for crystal growth were obtained from Aldrich in *Sure/Seal* bottles. Column chromatography was performed on silica gel 60 (ICN biomedicals 32−63 μm).

^{1}H NMR and ^{13}C NMR were performed on Bruker AC-200, AF-300, or Varian Inova 400 at 25 °C. All chemical shifts are given in ppm relative to $(CH_3)_4Si$ (0 ppm, ^{1}H), $CDCl_3$, (77.0 ppm, ^{13}C), and DMSO-d_6, (39.5 ppm, ^{13}C).

Size exclusion chromatography (SEC) was performed at 45 °C on a line consisting of a M510 pump, a U6K universal injector, a UV 486 detector (all Waters), a differential refractive index detector (Milton Roy), and a Model 110 differential viscometer (Viscotek). The separation was achieved across a set of three 5 μm PSS SDV columns (Polymer Standards Service) with porosities of 100 Å, 1000 Å, and Mixed C. The mobile phase was THF eluting at a normal flow rate of 1 mL/min. The molecular weight characteristics of the polymers were calculated by a polystyrene calibration curve constructed with 36 monodisperse polystyrene standards.

Powder X-ray diffraction data were recorded on an Enraf-Nonius Guinier Camera at 40 kV, 13 mA, or an Inel MPD diffractometer

(42) Sawaki, T.; Dewa, T.; Aoyama, Y. *J. Am. Chem. Soc.* **1998**, *120*, 8539.
(43) Sawaki, T.; Aoyama, Y. *J. Am. Chem. Soc.* **1999**, *121*, 4793.
(44) Miller, S. A.; Kim, E.; Gray, D. H.; Gin, D. L. *Angew. Chem., Int. Ed. Engl.* **1999**, *38*, 3022.
(45) Endo, K.; Koike, T.; Sawaki, T.; Hayashida, O.; Masuda, H.; Aoyama, Y. *J. Am. Chem. Soc.* **1995**, *117*, 8341.
(46) Fujita, M.; Kwon, Y. J.; Washizu, S.; Ogura, K. *J. Am. Chem. Soc.* **1994**, *116*, 1151.
(47) Toda, F.; Tanaka, K.; Miyahara, I.; Atsutsu, S.; Hirotsu, K. *Chem. Commun.* 1994, 1795.
(48) Korkas, P. P.; Weber, E.; Czugler, M.; Náray-Szabó, G. *Chem. Commun.* **1995**, 2229.
(49) Marjo, C. E.; Bishop, R.; Craig, D.; O'Brien, A.; Scudder, M. L. *Chem. Commun.* **1994,** 2513.
(50) Fujita, I.; Teki, Y.; Takui, T.; Kinoshita, T.; Itoh, K.; Miko, F.; Sawaki, Y.; Iwamura, H.; Izuoka, A.; Sugawara, T. *J. Am. Chem. Soc.* **1990**, *112*, 4074.
(51) Real, R. A.; Munno, G. D.; Muñoz, M. C.; Julve, M. *Inorg. Chem.* **1991**, *30*, 2701.
(52) Munno, G. D.; Julve, M.; Nicolo, F.; Lloret, F.; Faus, J.; Ruiz, R.; Sinn, *E. Angew. Chem., Int. Ed. Engl.* **1993**, *32*, 613.
(53) Karasawa, S.; Sano, Y.; Akita, T.; Koga, N.; Itoh, T.; Iwamura, H.; Rabu, P.; Drillon, M. *J. Am. Chem. Soc.* **1998**, *120*, 10080.
(54) Kou, H. Z.; Bu, W. M.; Liao, D. Z.; Jiang, Z. H.; Yan, S. P.; Fan, Y. G.; Wang, G. L. *J. Chem. Soc., Dalton Trans.* **1998**, 4161.
(55) Zhao, H.; Heintz, R. A.; Ouyang, X.; Dunbar, K. R.; Campana, C. F.; Rogers, R. D. *Chem. Mater.* **1999**, *11*, 736.
(56) Monfort, M.; Resino, I.; Ribas, J.; Stoeckli-Evans, H. *Angew. Chem., Int. Ed. Engl.* **2000**, *39*, 191.
(57) J6rome, D.; Mazaud, A.; Ribault, M.; Bechgaard, K. *J. Phys. Lett.* **1980**, *41*, L-95.
(58) Williams, J. M.; Beno, M. A.; Wang, H. H.; Leung, P. C. W.; Emge, T. J.; Geiser, U.; Carlson, K. D. *Acc. Chem. Res.* **1985**, *18*, 261.
(59) Tanigaki, K.; Ebbesen, T. W.; Saito, S.; Mizuki, J.; Tsai, J. S.; Kubo, Y.; Kurosh-ioma, S. *Nature (London)* **1991**, *352*, 222.
(60) Rosseinsky, M. J.; Murphy, D. W.; Fleming, R. M.; Zhou, O. *Nature (London)* **1993**, *364*, 425.
(61) Mitzi, D. B.; Feild, C. A.; Harrison, W. T. A.; Guloy, A. M. *Nature (London)* **1994**, *369*, 467.
(62) Batail, P.; Boubekeur, K.; Fourmigué, M.; Gabriel, J.-C. P. *Chem. Mater.* **1998**, *10*, 3005.
(63) Mitzi, D. B.; Wang, S.; Feild, C. A.; Chess, C. A.; Guloy, A. M. *Science* **1995**, *267*, 1473.
(64) Tang, Z.; Guloy, A. M. *J. Am. Chem. Soc.* **1999**, *121*, 452.
(65) Heintz, R. A.; Zhao, H.; Ouyang, X.; Grandinetti, G.; Cowen, J.; Dunbar, K. R. *Inorg. Chem.* **1999**, *38*, 144.
(66) Lehn, J.-M. *Supramolecular Chemistry: Concepts and Perspectives*; VCH: New York, 1995; p 141.
(67) Hönle, W.; Dettlaf-Weglikowska, U.; Walz, L.; von Schnering, H. G. *Angew. Chem., Int. Ed. Engl.* **1989**, *28*, 623.
(68) Burkett, S. L.; Sims, S. D.; Mann, S. *Chem. Commun.* **1996**, 1367.
(69) Lim, M. H.; Blanford, C. F.; Stein, A. **1997**, *119*, 4090.
(70) Cauvel, A.; Renard, G.; Brunel, D. *J. Org. Chem.* **1997**, *62*, 749.
(71) Feng, X.; Fryxell, G. E.; Wang, L.-Q.; Kim, A. Y.; Liu, J.; Kemner, K. M. *Science* **1997**, *276*, 923.
(72) Inagaki, S.; Guan, S.; Fukushima, Y.; Ohsuna, T.; Terasaki, O. *J. Am. Chem. Soc.* **1999**, *121*, 9611.
(73) Melde, B. J.; Holland, B. T.; Blanford, C. F.; Stein, A. *Chem. Mater.* **1999**, *11*, 3302.
(74) Lim, M. H.; Stein, A. *Chem. Mater.* **1999,** *11*, 3285.

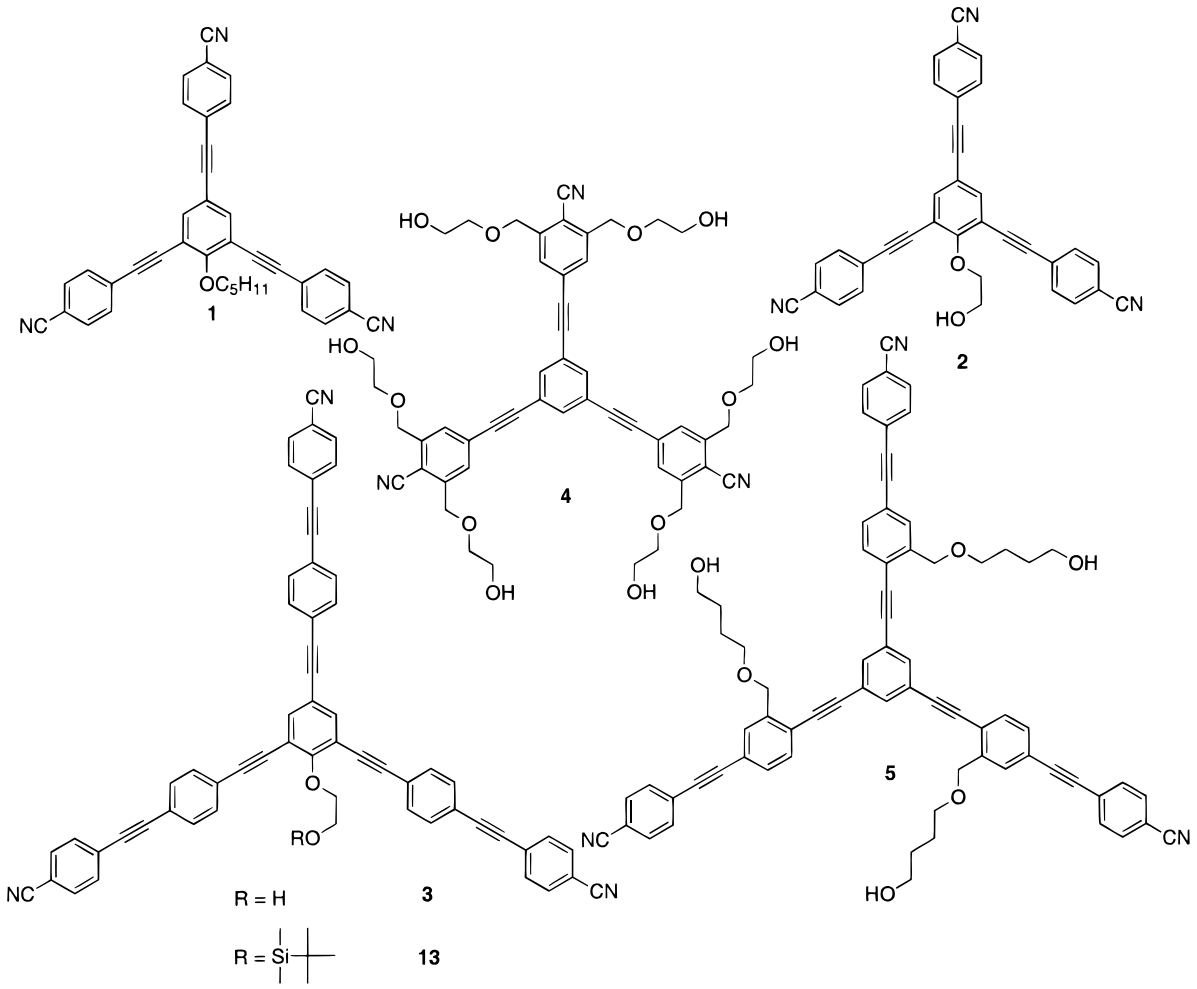

Figure 1. Tritopic phenylacetylene nitrile ligands **1**−**5** and **13**. **1** has a pentoxy side chain, **2**−**5** have hydroxy side chains, and **13** has a silyl ether side chain.

equipped with a CPS 120 detector at 20 kV, 15 mA, for Cu $K\alpha_1$; λ = 1.5406 Å. $RbZn_4Ga_5S_{12}$[75] was used as internal standard for the Guinier camera while for the Inel diffractometer a mixture of silver bohenate[76] and silicon was used as an external standard. Lattice constants were fitted and powder data were indexed by a least-squares method. Thermogravimetric analysis (TGA) was performed on a SEIKO Thermo-Gravimetric Differential Thermal Analyzer (TG/DTA 220) under nitrogen flow and at a rate of 20 deg/min.

2-(2,4,6-Tris(4-(trimethylsilylethynyl)phenylethynyl)phenoxy)-ethanol (6). A Schlenk flask equipped with a magnetic stirrer was charged with (2,4,6-tris(trimethylsilylethynyl)phenoxy)ethanol (10.5 g, 0.026 mol) and tetrahydrofuran (50 mL). The mixture was capped with a septum, evacuated, back-filled with nitrogen three times, and cooled to 5 °C in an ice bath. A 1.0 M solution of tetrabutylammonium fluoride in 9:1 tetrahydrofuran−water (5.0 mL, 5.0 mmol) was added rapidly via syringe. After 5 min the solution was concentrated to near dryness under reduced pressure on a rotary evaporator and the residue was eluted with chloroform through a plug of silica gel. The combined filtrate was evaporated to dryness under reduced pressure on a rotary evaporator and transferred to a heavy-walled Schlenk flask equipped with a magnetic stirrer. To this flask was added (4-bromophenylethynl)-trimethylsilane[77] (20.8 g, 0.0082 mol), copper(I) iodide (0.145 g, 0.76 mmol), triphenylphosphine (0.804 g, 3.1 mmol), bis(triphenylphosphine)palladium(II) chloride (0.539 g, 0.77 mmol), and triethylamine (250 mL). The flask was capped with a septum, evacuated, back-filled with nitrogen three times, sealed with a Teflon screw cap, and stirred at 80−90 °C overnight. The reaction mixture was then allowed to cool to room temperature and filtered through a fritted glass funnel. The filtrate was evaporated to dryness under reduced pressure on a rotary evaporator and the residue was purified by column chromatography on silica gel (1:1 dichloromethane−hexanes) to yield **6** as a yellow solid (9.84 g, 50%): ^{1}H NMR(200 MHz, acetone-d_6 δ 7.72−7.48 (m, 14H), 4.50 (t, J = 4.8 Hz, 2H), 3.99 (t, J = 4.8 Hz, 2H), 0.25 (s, 27H). ^{13}C NMR(100 MHz, acetone-d_6) δ 213.5, 137.1, 132.7, 132.4, 124.3, 124.1, 123.8, 123.7, 119.5, 118.9, 105.2, 97.0, 96.9, 94.9, 90.1, 87.1, 77.1, 62.3, 0.06, 0.05.

4-Bromo-2,6-bis((2-hydroxyethoxy)methyl)benzonitrile (7). To a solution of ethylene glycol (3.1 g, 0.05 mol) in anhydrous tetrahydrofuran (30 mL) was added sodium hydride (60% dispersion in mineral oil, 0.23 g, 5.6 mmol) in an ice bath over a period of 5 min. After the hydrogen gas stopped evolving, a solution of 4-bromo-2,6-bis(bromomethyl)benzonitrile[78] (10.6 g, 0.028 mol) in anhydrous tetrahydrofuran (10 mL) was added. The mixture was allowed to stir for 15 min at room temperature, poured into HCl (3 M, 30 mL), and extracted with ether (3 × 75 mL). The combined organic layer was dried over Na_2SO_4, evaporated under reduced pressure, and purified by column chromatography on silica gel (1:4 dichloromethane−ethyl acetate) to yield **7** as a white solid (0.81 g, 90%): ^{1}H NMR (300 MHz, $CDCl_3$) δ 7.68 (s, 2H), 4.73 (s, 4H), 3.86−3.82 (m, 4H), 3.73−3.71 (m, 4H). ^{1}H NMR (200 MHz, DMSO-d_6) δ 7.82 (s, 2H), 4.67 (s, 4H), 3.55 (s, 8H). ^{13}C NMR (75 MHz, $CDCl_3$) δ 144.3, 131.0, 128.4, 115.6, 109.1, 72.8, 70.5, 52.0.

(75) Schwer, H.; Keller, E.; Krämer, V. Z. *Z. Kristallogr.* **1993,** *204*, 203.

(76) Blanton, T. N.; Huang, T. C.; Toraya, H.; Hubbard, C. R.; Robie, S. B.; Louër, D.; Göbel, H. E.; Will, G.; Gilles, R.; Raftery, T. *Powder Diffraction* **1995**, *10*, 91.

(77) Steinmetz, M. G.; Yu, C.; Li, L. *J. Am. Chem. Soc.* **1994**, *116*, 932.

(78) Xu, Z.; Kiang, Y.-H.; Lee, S.; Lobkovsky, E.; Emmott, N. *J. Am. Chem. Soc.* Submitted for publication.

1-Bromo-4-iodo-2-methylbenzene (8). A suspension of 4-bromo-3-methylaniline (9.3 g, 0.05 mol) in 6 M HCl (200 mL) was stirred and heated at 90−95 °C in an Erlenmeyer flask for 1.5 h. The mixture was then cooled to 0 °C with an ice-bath. A solution of $NaNO_2$ (3.9 g, 56.5 mmol) in water (18 mL) was added dropwise with stirring to the reaction mixture. The mixture was stirred at 0 °C for aother 30 min, then added to a stirred solution of KI (83.5 g, 0.5 mol) in water (138 mL). After the reaction mixture was stirred overnight at room temperature, 1 M $Na_2S_2O_3$ (150 mL) was added. The mixture was extracted with ether (3 × 100 mL) and dried over Na_2SO_4. Column chromatography on silica gel (hexanes) afforded **8** as a colorless liquid (11 g, 74%): ^{1}H NMR (300 MHz, $CDCl_3$) δ 7.55 (d, J = 2.2 Hz, 1H), 7.33 (dd, J = 8.6, 2.2 Hz, 1H), 7.22 (d, J = 8.6 Hz, 1H), 2.3 (s, 3H). ^{13}C NMR (75 MHz, $CDCl_3$) δ 140.2, 139.4, 136.2, 133.9, 124.7, 92.3, 22.6. GC-MS m/z 298 (M + 1), 296 (M − 1).

1-Bromo-2-bromomethyl-4-iodobenzene (9). A heavy-walled Schlenk flask was charged with **8** (10.2 g, 0.035 mol), *N*-bromosuccinimide (9.5 g, 0.053 mol), and benzoyl peroxide (60 mg, 0.25 mmol). The mixture was evacuated, back-filled with nitrogen, sealed with a Teflon cap, and stirred at 80 °C for 24 h. After being cooled to room temperature, the mixture was poured into 5% $NaHSO_3$ (120 mL), extracted with ether (3 × 75 mL), and then dried over Na_2 SO_4. Recrystallization from hot hexanes afforded **9** as white crystals (8.1 g, 62%): ^{1}H NMR (300 MHz, $CDCl_3$) δ 7.75 (d, J = 2.15 Hz, 1H), 7.44 (dd, J = 8.6, 2.15 Hz, 1H), 7.27 (d, J = 8.6 Hz, 1H), 4.48 (s, 3H). ^{13}C NMR (75 MHz, $CDCl_3$) δ 139.8, 139.2, 139.0, 134.8, 124.2, 92.4, 31.9.

4-(2-Bromo-5-iodobenzyloxyl)butan-1-ol (10). To a solution of 1,4-butadiol (25 g, 0.28 mol) in anhydrous tetrahydrofuran (30 mL) was added sodium hydride (60% dispersion in mineral oil, 1.34 g, 0.033 mol) in an ice bath over a period of 5 min. After the suspension was stirred for another 10 min in an ice-bath, a solution of **9** (10.6 g, 0.028 mol) in anhydrous tetrahydrofuran (10 mL) was added to the suspension. The mixture was then stirred for 2 h at 60 °C. After the reaction mixture was cooled to room temperature, it was added to HCl (3 M, 100 mL) and extracted with ether (3 × 75 mL). The combined organic layer was dried over Na_2SO_4, evaporated under reduced pressure, and purified by column chromatography on silica gel (4:1 dichloromethane−ethyl acetate) to yield **10** as a viscous liquid (9.6 g, 89%): ^{1}H NMR (300 MHz, $CDCl_3$) δ 7.76 (d, J = 2.15 Hz 1H), 7.43 (dd, J = 8.3, 2.15 Hz, 1H), 7.22 (d, J = 8.3 Hz, 1H), 4.48 (s, 2H) 3.68 (t, J 5.9 Hz, 2H), 3.58 (t, J = 5.9 Hz, 2H), 1.74−1.67 (m, 4H). ^{13}C NMR (75 MHz, $CDCl_3$) δ 139.9, 137.8, 137.6, 134.5, 122.2, 92.6, 71.5, 71.0, 62.7, 29.8, 26.3.

4-(4-Bromo-3-((4-hydroxybutoxy)methyl)phenylethynyl)benzonitrile (11). A Schlenk flask was charged with **10** (7.54 g, 0.02 mol), 4-ethynylbenzonitrile (3.05 g, 0.02 mol), copper(I) iodide (38 mg, 0.2 mmol), triphenylphosphine (524 mg, 2.0 mmol), bis(dibenzylideneacetone)palladium(0) (214 mg, 0.4 mmol), and triethylamine (70 mL). The flask was capped with a septum, evacuated, back-filled with nitrogen, sealed with a Teflon cap, and heated at 50 °C for 16 h. The reaction mixture was then allowed to cool to room temperature and evaporated under reduced pressure on a rotary evaporator. The residue was purified by column chromatography on silica gel (2:1 hexanes−THF) to yield **11** as a beige solid (5.2 g, 70%): ^{1}H NMR (300 MHz, $CDCl_3$) δ 7.64−7.57 (m, 5H), 7.53 (d, J = 8.6 Hz, 1H), 7.26 (dd, J = 8.3, 2.15 Hz, 1H), 4.55 (s, 2H), 3.68 (t, J = 5.9 Hz, 2H), 3.62 (t, J = 5.9 Hz, 2H), 1.77−1.69 (m, 4H). ^{13}C NMR (75 MHz, $CDCl_3$) δ 138.3, 132.7, 132.1, 131.9, 131.8, 127.9, 123.5, 121.6, 118.5, 111.7, 92.8, 88.6, 71.8, 71.1, 62.7, 29.9, 26.4.

(2,4,6-Tris(4-((4-cyanophenyl)enthynyl)phenylethynyl)phenoxy)-ethanol (3). A Schlenk flask equipped with a magnetic stirrer was charged with **7** (5.0 g, 6.86 mmol), potassium carbonate (5.0 g, 36 mmol), and a methanol/dichloromethane 1−3 solution (50 mL) and stirred under nitrogen for 3 h at room temperature. The mixture was then transferred via syringe to a heavy-walled Schlenk flask. To this flask was added 4-bromobenzonitrile (4.36 g, 0.024 mol), copper(I) iodide (65 mg, 0.34 mmol), triphenylphosphine (0.227 g, 8.7 mmol), bis(triphenylphosphine)palladium(II) chloride (0.227 g, 0.0.32 mmol), and triethylamine (100 mL). The flask was capped with a septum, evacuated, back-filled with nitrogen three times, sealed with a Teflon screw cap, and stirred at 80−90 °C overnight. The reaction mixture was then allowed to cool to room temperature and filtered through a fritted glass funnel. The filtrate was evaporated to dryness under reduced pressure on a rotary evaporator and the residue was purified by column chromatography on silica gel (2:3 ethyl acetate−hexanes) to yield **3** as a yellow solid (4.53 g, 81%): IR (KBr, cm^{-1}) 2228, 2215, 1684, 1653, 1615, 1599, 1576, 1570, 1559, 1514, 1457, 1440, 1406, 1362, 1240, 1104, 1017, 836, 668, 539, 431, 422, 418, 411. 1H NMR (200 MHz, $CDCl_3$) δ 7.88−7.65 (m, 26H), 4.58 (t, J = 4.8 Hz, 2H), 4.04 (t, J = 4.8 Hz, 2H). ^{13}C NMR (100 MHz, $CDCl_3$) δ 162.2, 137.3, 133.1, 133.0, 132.7, 132.6, 132.5, 128.4, 124.5, 123.6, 123.4, 119.6, 119.1, 118.8, 113.1, 95.0, 93.5, 90.6, 90.4, 90.2, 87.6, 77.3, 62.4, 30.7, 25.7, 25.5, 25.3, 25.1, 24.9. HRMS-FAB (m/z) $[M + H]^+$ calcd 814.2495, found 814.2492.

1,3,5-Tris(4-cyano-3,5-bis((2-hydroxyethoxy)methyl)phenylethynyl)-benzene (4). A heavy-walled Schlenk flask was charged with **7** (0.21 g, 0.64 mmol), 1,3,5-triethynylbenzene (30 mg, 0.2 mmol), copper(I) iodide (3 mg, 15 μmol), triphenylphosphine (15 mg, 57 μmol), bis-(triphenylphosphine)palladium(II) chloride (10 mg, 14 μmol), and triethylamine (13 mL). The flask was capped with a septum, evacuated, and back-filled with nitrogen, sealed with a Teflon cap, and stirred at 85 °C for 16 h. The reaction mixture was then allowed to cool to room temperature and evaporated under reduced pressure on a rotary evaporator. The residue was purified by column chromatography on silica gel (5:1 ethyl acetate−triethylamine) to yield **4** as a palm yellow solid (0.14 g, 80%): ^{1}H NMR (300 MHz, DMSO-d_6) δ 7.95 (s, 3H), 7.79 (s, 6H), 4.71 (s, 12H), 3.59 (s, 24H). ^{13}C NMR (75 MHz, DMSO-d_6) δ 139.1, 126.2, 124.3, 122.0, 119.1, 111.0, 105.8, 86.8, 85.8, 68.6, 65.7, 56.3. HRMS (ES) m/z calcd 898.3551, found 898.3577.

1,3,5-Tris(4-((4-cyanophenyl)ethynyl)-2-((4-hydroxybutoxy)methyl)phenylethynyl)benzene (5). A heavy-walled Schlenk flask was charged with **11** (5.2 g, 0.014 mol), 1,3,5-triethynylbenzene (0.58 g, 3.8 mmol), copper(I) iodide (25 mg, 0.13 mmol), triphenylphosphine (350 mg, 1.34 mmol), bis(triphenylphosphine)palladium(II) chloride (189 mg, 0.27 mmol), and triethylamine (45 mL). The flask was capped with a septum, evacuated, and back-filled with nitrogen, sealed with a Teflon cap, and stirred at 75 °C for 36 h. The reaction mixture was then allowed to cool to room temperature and evaporated under reduced pressure on a rotary evaporator. The residue was purified by column chromatography on silica gel (2:1 ethyl acetate−CH_2 Cl_2) to yield **5** as a yellow solid (1.1 g, 27%): IR (KBr, cm^{-1}) 3387, 2634, 2853, 2228, 2210, 1600, 1579, 1505, 1121, 836. ^{1}H NMR (300 MHz, $CDCl_3$) δ 7.66−7.58 (m, 18H), 7.53 (d, J = 8.1 Hz, 3H), 7.45 (dd, J = 8.1, 1.6 Hz, 3H), 3.67 (d, J = 5.9 Hz, 6H), 3.64 (d, J = 5.9 Hz, 6H), 1.83−1.66 (m, 12H). ^{13}C NMR (75 MHz, $CDCl_3$) δ 140.6, 134.2, 132.3, 132.1, 130.8, 130.6, 127.8, 123.9, 122.8, 121.7, 118.4, 111.8, 94.0, 93.3, 89.7, 88.1, 71.0, 70.6, 62.6, 29.9, 26.6. HRMS-FAB (m/z) $[M + H]^+$ calcd 1060.4326, found 1060.4323.

***tert*-Butyl((2,4,6-tris((4-cyanophenyl)ethynyl)phenoxy)ethoxy)-dimethylsilane (12).** A heavy-walled Schlenk flask equipped with a magnetic stirrer was charged with **2** (10 mg, 1.9 μmol), *tert*-butyldimethylsilyl chloride (20 mg, 0.13 mmol), imidazole (20 mg, 0.29 mmol), and dichloromethane (15 mL) and stirred under nitrogen for 3 h at room temperature. The reaction flask was then charged with *tert*-butyldimethylsilyl chloride (20 mg, 0.13 mmol) and (dimethylamino)pyridine (20 mg, 1.6 mmol) and allowed to stir overnight. The reaction mixture was then washed with water (2 × 50 mL) and dried over magnesium sulfate, and the filtrate was evacuated to dryness to yield **12** as a yellow solid (100% by thin-layer chromatography). An alternative silylation reaction is as follows: A heavy-walled Schlenk flask equipped with a magnetic stirrer was charged with **2** (5 mg, 0.95 μmol), *tert*-butyldimethyltrifluoromethane sulfonate (30 mg, 0.11 mmol), 2,6-di-ert*t*-butylpyridine (50 mg, 0.26 mmol), and anhydrous benzene (3 mL) and stirred under nitrogen for 1 h at room temperature. After 1 h, thin-layer chromatography indicated complete conversion to **12**: ^{1}H NMR (200 MHz, DMSO-d_6) δ 7.97−7.73 (m, 14H), 4.53 (t, J = 4.8 Hz, 2H), 4.01 (t, J = 4.8 Hz, 2H), 0.74 (s, 9H), −0.36 (s, 6H). MS (EI, 70 eV) m/z 57 (11.1), 59 (12.5), 73 (36.2), 75 (28.2), 101 (15.7), 263 (29.4), 264 (15.3), 526 (100), 527 (45.8), 528 (15.8), 570 (74.3), 571 (37.4), 572 (12.7).

***tert*-Butyl((2,4,6-tris(4-((4-cyanophenyl)ethynyl)phenylethynyl)-phenoxy)ethoxy)dimethylsilane (13).** A heavy-walled Schlenk flask equipped with a magnetic stirrer was charged with **3** (0.498 g, 0.61

mmol), *tert*-butyldimethylsilyl chloride (92 mg, 0.61 mmol), (dimethylamino)pyridine (0.224 g, 1.8 mmol), and anhydrous tetrahydrofuran (50 mL) and stirred under nitrogen for 4 h at room temperature. The flask was again charged with *tert*-butyldimethylsilyl chloride (92 mg, 0.61 mmol) and (dimethylamino)pyridine (0.224 g, 1.8 mmol) and allowed to stir overnight. The reaction mixture was then evacuated to dryness on a rotary evaporator, and the residue was chromatographed on silica gel to yield **13** as a yellow solid (0.60 g, 100%). An alternative silylation reaction is as follows: A heavy-walled Schlenk flask equipped with a magnetic stirrer was charged with **3** (5 mg, 0.62 μmol), *tert*-butyldimethyltrifluoromethane sulfonate (30 mg, 0.11 mmol), 2,6-di-*tert*-butylpyridine (50 mg, 0.26 mmol), and anhydrous benzene (3 mL) and stirred under nitrogen for 1 h at room temperature. After 1 h, thin-layer chromatography indicated complete conversion to **13**: IR (KBr, cm^{-1}) 2953, 2928, 2902, 2895, 2882, 2856, 2362, 2228, 2215, 1600, 1514, 1440, 1106, 835, 666, 434, 421, 411, 394. ^{1}H NMR (200 MHz, acetone-d_6) δ 7.88−7.66 (m, 26H), 4.60 (t, J = 4.6 Hz, 2H), 4.17 (t, J = 4.8 Hz, 2H), 0.86 (s, 9H), 0.08 (s, 6H). ^{13}C NMR (100 MHz, THF-d_6) δ 160.9, 136.4. 131.9, 131.6, 131.5, 127.7, 12.35, 122.2, 122.0, 118.3, 117.6, 111.5, 93.9, 93.2, 93.1, 89.7, 89.6, 89.3, 86.8, 62.7, 25.9, 25.7, 18.2, −5.4. HRMS-FAB (m/z) $[M + H]^+$ calcd 928.3359, found 928.3353.

Di-*tert*-butylbis((2,4,6-tris(4-((4-cyanophenyl)ethynyl)phenylethynyl)phenoxy)ethoxy)silane (14). A heavy-walled Schlenk flask equipped with a magnetic stirrer was charged with **3** (0.405 g, 0.50 mmol), 2,6-di-*tert*-butylpyridine (0.852 g, 4.4 mmol), di-*tert*-butylsilyl bis(trifluoromethanesulfonate) (0.109 g, 0.25 mmol), and anhydrous tetrahydrofuran (5 mL) and the reaction mixture was stirred at room temperature overnight. Excess *tert*-butyldimethylsilyl chloride (>0.5 g, 3.3 mmol) was added and the mixture was stirred at room temperature for an additional 3 days. The tetrahydrofuran was then removed in vacuo, the residue dissolved in dichloromethane, and the insoluble solid separated by filtration. The filtrate was then evaporated to dryness on the rotary evaporator and the solid was washed with a minimum of cold acetone (3 × 5 mL), leaving behind **14** as a yellow solid (0.29 g, 33%): IR (KBr cm^{-1}) 3068, 2935, 2861, 2228, 2215, 1599, 1558, 1514, 1473, 1456, 1437, 1406, 1271, 1136, 1106, 1031, 1017, 834, 730. ^{1}H NMR (200 MHz, acetone-d_6) δ 7.88−7.52 (m, 52H), 4.59 (t, J = 5.2 Hz, 4H), 4.17 (t, J = 5.2 Hz, 4H), 1.11 (s, 18H). ^{13}C NMR (100 MHz, $CDCl_3$) δ 217.7, 160.7, 154.0, 144.1, 136.4, 131.9, 131.8, 131.6, 131.5, 131.4, 131.3, 127.6, 124.3, 123.3, 122.1, 118.2, 117.4, 111.6, 93.9, 93.2, 93.1, 89.7, 89.6, 89.5, 89.3, 86.9, 27.8, 27.4, 21.1, 21.1. MS (FAB) m/z 1768 $[M + H]^+$.

Di-*tert*-butyl(2,4,6-tris((4-((4-cyanophenyl)ethynyl)phenylethynyl)-phenoxy)ethoxy)silanol (15). A heavy-walled Schlenk flask equipped with a magnetic stirrer was charged with **3** (0.100 g, 0.013 mmol), 2,6-di-*tert*-butylpyridine (0.50 g, 2.9 mmol), di-*tert*-butylsilyl bis-(trifluoromethanesulfonate) (0.50 g, 1.1 mmol), and anhydrous tetrahydrofuran (5 mL) and the reaction mixture was allowed to stir overnight at room temperature. The flask was then charged with water (300 mL), the mixture was evaporated to dryness on a rotary evaporator, and the residue was placed in a sublimator under vacuum at 80 °C. After the crystalline byproduct was removed by sublimation, the flask was cooled and the residue was recovered to yield **15** (60 mg, 46%): IR (KBr cm^{-1}) 3484, 3416, 2962, 2932, 2856, 2227, 2216, 1599, 1515, 1439, 1260, 1108, 835. ^{1}H NMR (200 MHz, acetone-d_6) δ 7.81−7.67 (m, 26H), 5.18 (s, 1H), 4.67 (t, J = 5.4 Hz, 2H), 4.34 (t, J = 5.4 Hz, 2H), 0.98 (s, 18H). MS (FAB) m/z 972 (M^+).

Preparation of Microcrystalline Powders 2·AgOTf. To a solution of **2** (0.3 g, 0.37 mmol) in anhydrous benzene (15 mL) was added a solution of silver(I) trifluoromethanesulfonate (0.1 g, 0.37 mmol) in anhydrous benzene (15 mL) in a vial with a Teflon-lined screw cap. This vial was then placed in a furnace equipped with an Eurotherm temperature controller and heated from room temperature to 98 °C at 0.5 deg/min, held at 98 °C for 60 min, then slowly cooled to room temperature at 0.02°Cdeg/min to yield crystalline powder.

Preparation of Microcrystalline Powders 3·AgOTf. In a glovebox with argon atmosphere, a solution of silver(I) trifluoromethanesulfonate (25 mg, 0.1 mmol) in anhydrous benzene (1 mL) was added to a solution of **3** (40 mg, 0.1 mmol) in anhydrous benzene (1 mL) in a vial. Upon addition white precipitate formed immediately. Anhydrous acetonitrile (0.3 mL) was then added to the vial to dissolve the white solids. The vial was then left undisturbed and exposed to the argon atmosphere to allow escape of solvent. Crystalline precipitate formed after 24 h.

Preparation of Microcrystalline Powders 4·AgOTf. 4 (4.5 mg, 5.0 μmol) was dissolved in acetone (1.0 mL) in a capped vial heated in an oil-bath at 50 °C. The vial was then taken out of the bath and a solution of silver(I) trifluoromethanesulfonate (1.3 mg, 5.0 μmol) in benzene (1.0 mL) was added. The mixture was allowed to cool to room temperature to yield crystalline powder.

Preparation of Microcrystalline Powders 5·AgOTf. To a solution of **5** (30 mg, 0.03 mmol) in anhydrous benzene (8 mL) was added a solution of silver(I) trifluoromethanesulfonate (8 mg, 0.03 mmol) in anhydrous benzene (2 mL) in a Schlenk flask sealed with a Teflon-lined screw cap. This flask was then placed in a furnace equipped with an Eurotherm temperature controller and heated from room temperature to 110 °C at 0.5 deg/min, held at 110 °C for 70 min, then slowly cooled to room temperature at 0.02 deg/min to yield crystalline powder.

Preparation of Microcrystalline Powders 13·AgOTf. To a solution of **13** (20 mg, 0.02 mmol) in benzene (1.8 mL) was added silver(I) trifluoromethanesulfonate (5 mg, 0.02 mg) in benzene (1 mL) in a vial with a Teflon-lined screw cap. This vial was then placed in a furnace equipped with an Eurotherm temperature controller and heated from room temperature to 98 °C at 0.5 deg/min, held at 98 °C for 70 min, then slowly cooled to room temperature at 0.1 deg/min to yield crystalline powder.

Solid State Monosilylation of 3·AgOTf. The crystalline powder sample **3**·AgOTf (50 mg, 0.06 mmol) grown in anhydrous benzene was exposed to 2,6-di-*tert*-butylpyridine (0.3 g, 1.6 mmol) and *tert*-butyldimethylsilyl (trifluoromethanesulfonate) (60 mg, 0.05 mmol) in a glovebox. After 3 days, a small amount of the reaction mixture was sealed in a 1.0 mm special glass capillary tube, removed from the glovebox, and mounted on a Guinier camera for X-ray diffraction pattern collection. Another small amount of the reaction mixture was filtered and removed from the glovebox. This sample was then placed on a vacuum line for 2 h, quenched with ethanol to further remove any possible unreacted *tert*-butyldimethylsilyl bis(trifluoromethanesulfonate), and dissolved in acetone-d_6 for ^{1}H NMR characterization. To the remaining reaction mixture in the glovebox was added 2,6-di-*tert*-butylpyridine (0.3 g, 1.6 mmol), and *tert*-butyldimethylsilyl (trifluoromethanesulfonate) (60 mg, 0.05 mmol). The reaction mixture was stirred for a week. It was filtered, removed from the glovebox, placed on vacuum line for 2 h, quenched with ethanol, and was then divided into two portions. One portion was dissolved in acetone-d_6 for ^{1}H NMR characterization. A second portion of the reaction mixture was again filtered and washed thoroughly with water, and a small sample was sealed in a special glass capillary tube for X-ray powder pattern collection.

Solid State Disilylation of 3·AgOTf. The crystalline powder sample **3**·AgOTf (300 mg, 0.37 mmol) grown in anhydrous benzene was placed in a Schlenk tube capped with a septum. The reaction tube was evacuated and back-filled with nitrogen and 2,6-di-*tert*-butylpyridine (0.7 g, 3.7 mmol) and di-*tert*-butylsilyl bis(trifluoromethanesulfonate) (82 mg, 0.19 mmol) were added via syringe. The septum was then replaced by a Teflon-lined screw cap and the reaction mixture stirred under nitrogen. After a week, a small portion of the reaction mixture was removed from the Schlenk tube, filtered, washed thoroughly with water, and dissolved in acetone-d_6 for ^{1}H NMR characterization. The remaining reaction mixture was stirred under nitrogen for another week, then monitored with ^{1}H NMR again. After verifying by ^{1}H NMR that **3** had reacted completely, the reaction mixture was filtered and the solid was washed with water. A portion of the solid thus obtained was then sealed in a 1.0 mm special glass capillary tube and mounted on an X-ray diffractometer for powder pattern collection.

Solid State Polymerization of 5·AgOTf. The crystalline powder sample of **5**·AgOTf (62 mg, 0.047 mmol) grown in anhydrous benzene was placed in a Schlenk tube capped with a septum. The reaction tube was evacuated and back-filled with nitrogen and 2,6-di-*tert*-butylpyridine (46 mg, 0.24 mmol) and di-*tert*-butylsilyl bis(trifluoromethanesulfonate) (31 mg, 0.07 mmol) was added via syringe. The septum was then replaced by a Teflon-lined screw cap. The reaction

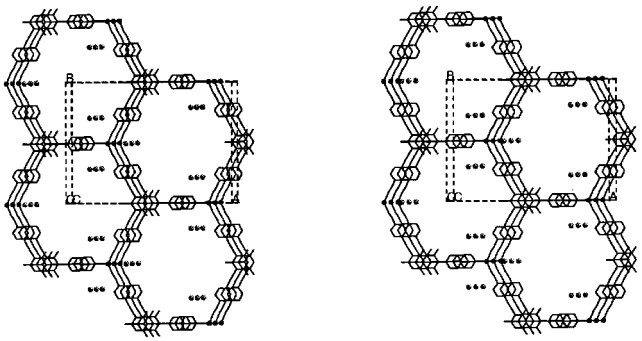

Figure 2. Stereoview of the single-crystal structure of **1**·AgOTf. Silver atoms are represented as black spheres and sulfur atoms as gray spheres.

flask was again evacuated and back-filled with nitrogen, then stirred at room temperature. The course of this solid state reaction was monitored by size exclusion chromatography. After 3 weeks of stirring at room temperature under nitrogen, the reaction mixture was filtered, washed thoroughly with water, and divided into two portions. The first portion was sealed in a 1.0 mm special glass capillary tube and mounted on an X-ray diffractometer for powder pattern collection. The second portion was dissolved in tetrahydrofuran (10 mg to 1 mL) for size exclusion chromatography.

Vapor Exchange of Polymerized 5·AgOTf. The polymerized **5**·AgOTf was placed in a thermogravimetric analyzer and heated to 150 °C at a rate of 20 deg/min to void the solid of initially included solvent. The apohost was then suspended above a solution of toluene molecules, taking care to maintain spatial separation between host and guest, and sealed in a vial. The vial was heated to 50 °C for 48 h. The sample was then analyzed by both TGA and X-ray powder diffraction.

Results and Discussion

In earlier work[11,26,78,79] we have explored the crystalline structure of 3-fold symmetric phenylacetylene nitriles and silver triflate complexes. From a study of 20 such systems (including eight single-crystal structures), a common structural theme has emerged. In all cases such 3-fold symmetric molecules form a honeycomb extended network in which every organic molecule is bonded to three silver ions and each silver ion is trigonally planar coordinated to three organic molecules. A typical single-crystal **1**·AgOTf is illustrated in Figure 2. Its corresponding X-ray powder diffraction pattern is shown in Figure 3c. In this crystal structure, parallel layers of a two-dimensional honeycomb network are stacked along the *c* axis. The interlayer distance is 3.52 Å. This *c* axis is not normal to the *ab* plane of the crystal. Instead, as can be seen in Figure 2, the individual honeycomb sheets are rotated out of the normal plane by a small rotation. The *b* axis is the axis of rotation. Had there been no such rotation, all the axes could be mutually orthogonal and the unit cell would have appeared orthorhombic. This orthorhombic cell would have a *b/a* ratio of $\sqrt{3}$ as it is a *C*-centered super-cell corresponding to a hexagonal primitive cell. With the observed rotation the *b* axis remains unchanged, the *a* axis becomes significantly shorter, α and β stay at 90°, and the resulting crystal is monoclinic.

Each of these structural features affects the resulting powder pattern. Most important is the interlayer spacing of 3.52 Å. This distance corresponds to a 2 θ angle (Cu $K\alpha$ radiation) of 25.3°, hence all powder pattern reflections below this angle are due to *hk*0 reflections. As Figure 3 shows, the predominant *hk*0 reflections, *110* and *200*, partially fuse together to form the largest reflection, a reflection significantly more intense than any other. The strength of this reflection is due to the contrast in crystallinity and electron density of the channel walls as

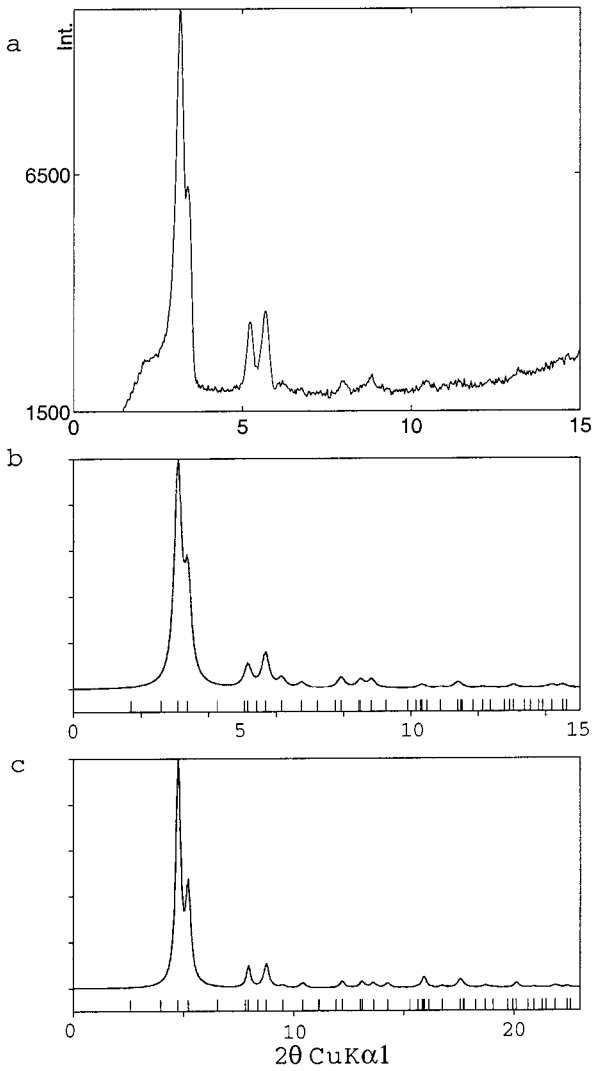

Figure 3. (a) Observed and (b) calculated X-ray diffraction patterns for **3**·AgOTf. (c) Calculated X-ray diffraction pattern based on the single-crystal structure of **1**·AgOTf.

opposed to the channel interior. Large *110* and *200* peaks are the hallmark of a channel type porous solid. Finally, in Figure 3c, it can be observed that while diffraction peaks appear to be fused double peaks at low angle, at higher angles these double peaks resolve into separate but closely spaced signals. This splitting is due to the rotation of the honeycomb sheets away from the plane normal to the *c* axis, and the consequent lowering of the unit cell symmetry from hexagonal to monoclinic.

3·AgOTf. The X-ray powder pattern of **3**·AgOTf is shown in Figure 3a. Shown here are the low-angle features. The full powder data set is given in the Supporting Information. The similarity between this powder pattern and the one in Figure 3c based on the single-crystal data is clear. There are, however, two notable differences. First it may be seen that near 15° there is the onset of an extremely broad feature. This feature can be attributed to diffraction from the benzene solvent in which the sample was immersed during data collection. Second, the 2θ angle scales of the two patterns are different. This difference in diffraction angles can be understood if one notes the difference in size of the organic molecules in the two samples. Compared to **1**, the organic molecule **3** has an additional three aromatic rings. This larger size results in a larger real space unit cell, smaller reciprocal lattice cell, and correspondingly smaller 2θ angles for equivalent reflections.

(79) Choe, W.; Kiang, Y.-H.; Xu, Z.; Lee, S. *Chem. Mater.* **1999**, *11*, 1776.

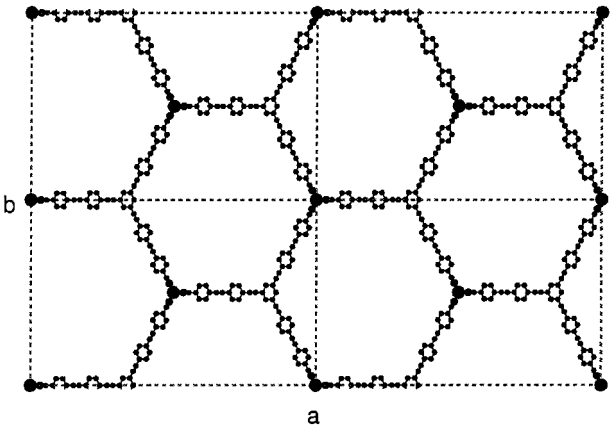

Figure 4. View down the channel direction of the model structure for **3**·AgOTf. The calculated diffraction pattern in Figure 3c is based on this model. Large spheres, Ag; medium spheres, N; small spheres, C.

Recalling that data with 2θ angles less than 25° are *hk*0 reflections, we refined the low-angle data given in Figure 3a and the Supporting Information to a two-dimensional *C*-centered rectangular cell. This projected rectangular cell was refined to an $a = 52.37(9)$ Å and $b = 33.99(4)$ Å. Given the low-angle nature of the data and the comparatively large cell constants of these data, the low standard deviation suggests the validity of this rectangular cell. We further note the honeycomb net illustrated in Figure 2 is based on a rigid hexagonal net of organic molecules linked to silver ions. Using knowledge of the molecular structure of **3**, tabulated bond lengths,[80] and an Ag−N bond distance of 2.2 Å, we find the calculated distance for the Ag ions to the centroid of the central aromatic ring in **3** to be 19.9 Å. This corresponds to a *b* axis of 34 Å, in good agreement with the experimentally observed value.

Following the single-crystal model illustrated in Figure 2, we use the *b* axis as an axis of rotation to rotate these rigid hexagonal nets. In this way we generated an *a* axis corresponding to the experimentally observed *a* axis of 52.4 Å. This provides us with the necessary data to generate the crystal model shown in Figure 4. The atomic coordinates of this model are given in the Supporting Information. As in the initial crystal structure illustrated in Figure 2, only the rigid backbone, the Ag ions, and the sulfur atoms of the triflate ions are located. Even though solvent, the alkoxy side chains, and the remaining triflate atoms are not included, nor has there been refinement of any atomic parameters, the powder pattern generated from this model (see Figure 3b) is reasonably similar to the pattern found experimentally (Figure 3a). While the angular resolution of our data is only 4 Å, this length is significantly smaller than the channel diameters of 20−30 Å and therefore the data support the presence of channels in the structure. Finally, as we have only two reflections which correspond to *hkl* ($l \neq 0$), it seemed prudent to consider here only the projection of the crystal structure onto the two-dimensional plane normal to the *c* axis.

We base the validity of our structural assignment on three points. First, the observed powder pattern is similar to those found in previously studied single-crystal structures. In the inorganic solid state literature this is generally considered proof of an isotypic structure. Second, the observed lattice constants are in agreement with the cell constants of a chemically reasonable model based on standard organic bond lengths. Finally, the generation of a crystal model based on this proposed structure leads to a powder pattern similar to the one observed experimentally even in the absence of atomic parameter refinement.

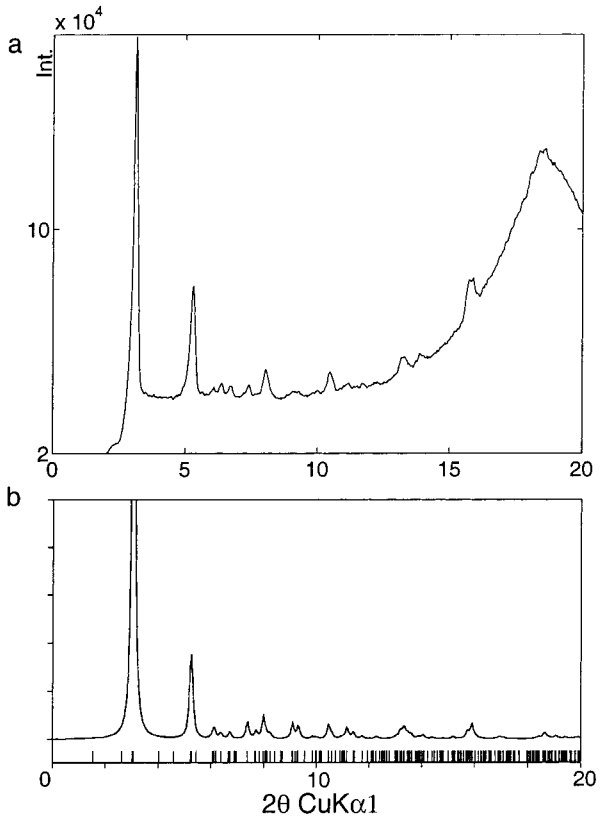

Figure 5. (a) Observed and (b) calculated X-ray diffraction patterns for **5**·AgOTf.

5·AgOTf. The X-ray powder pattern of **5**·AgOTf is shown in Figure 5. It may be seen that while this powder pattern retains many features in common with the earlier powder patterns, the splitting between pairs of peaks is significantly smaller. Only at higher angles can one see the separation between pairs. Besides the main reflections, a number of weak reflections also appear. These additional reflections suggest that the crystal has a super-cell, caused by the stacking pattern of honeycomb layers on top of one another. We were able to refine the 31 observed reflections into a monoclinic cell with $a = 59.46(6)$ Å, $b = 33.81(2)$ Å, $c = =14.283(7)$ Å, and $\beta = 103.8(1)°$. The refinement is given in the Supporting Information. Given the low angles in the observed data as well as the large unit cell lengths, the small standard deviations in cell lengths strongly support the validity of this refined cell. The systematic absences found in these reflections suggest the crystal is in the *C*2, *Cm*, or *C*2/*m* space group.[81]

The *b* axis length of 33.81 Å is in substantial agreement with the 34 Å axis estimated from tabulated organic bond lengths and the *b* axis of 33.99 Å found in **3**·AgOTf. The *c* axis of 14.28 Å is four times 3.57 Å, suggesting a stacking of four layers within the unit cell. We have seen such 4-fold stacking sequences in our earlier single-crystal structures. These earlier structures showed that in such cases the layers shift with respect to one another so that the triflate ions, which are coordinated to the Ag atoms, lie in the cleft of the adjacent layers either above or beneath them in the stacking sequence. Furthermore, the layers stack in such a way as to place as many aromatic

(80) March, J. *Advanced Organic Chemistry*, 4th ed.; Wiley: New York, 1992; p 21.

(81) Hahn, T., Ed. *International Tables for Crystallography*, 4th revised ed.; Kluwer Academic Publishers: Boston, 1995; Vol. A.

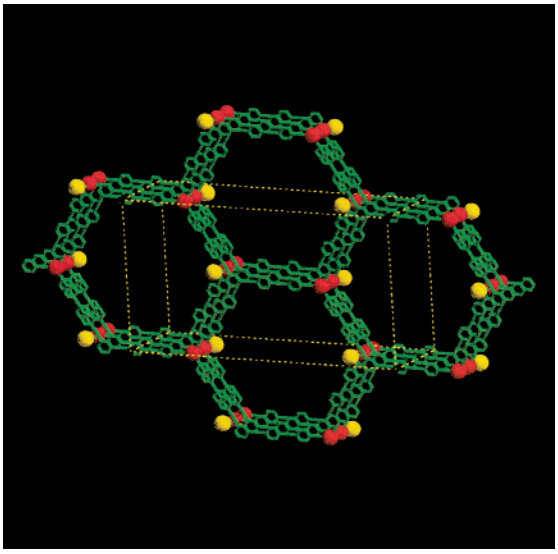

Figure 6. View down the channel direction of the model structure for **5**·AgOTf. The calculated diffraction pattern in Figure 5b is obtained from this model. Molecule **5** is shown in green, silver in red, and sulfur in yellow.

rings as possible on top of each other in a staggered arrangement. We therefore constructed a model using these facts. We chose to place the model in *C*2/*m* symmetry, not just because for extended solids it is the most common of the three possible space groups,[82] but also because it seemed pointless not to assume the presence of an inversion center. This inversion center enforces a pairing of the honeycomb layers in which the triflate ions of neighboring layers lie in the cleft of the adjacent pair. The staggering of the aromatic rings and the *C*2/*m* mirror plane symmetry dictate how these pairs lie with respect to neighboring pairs. The constructed model is shown in Figure 6. The atomic coordinates for this model are given in the Supporting Information. In this model the triflate ions are represented by the sulfur atoms and the bridging oxygen atoms. The resultant powder pattern is shown in Figure 5b. The agreement between calculated and observed patterns is reasonably good. This agreement is of special interest as no atomic parameters were refined to improve the agreement. Furthermore, the side chains, the remaining triflate components, and solvent molecules were not located in our model and hence their influence on peak intensities could not be assessed.

4·AgOTf. The X-ray powder pattern of **4**·AgOTf is illustrated in Figure 7. Shown here are the low-angle features. The full powder data set is given in the Supporting Information. The observed powder pattern bears several features in common with the previously discussed ones. The principal reflection is found at the lowest angle, followed by four or five smaller peaks. A broad feature attributable to the solvent benzene is found for 2θ values between 15 and 25°. As in **5**·AgOTf, the splitting between pairs of peaks is quite small. Even at higher angles there is no clear evidence of irregular peak shape. We therefore refined the data with a two-dimensional hexagonal cell with an *a* axis of 22.30(5) Å. This refinement is given in the Supporting Information. This *a* axis is in substantial agreement with that obtained using standard bond lengths as well as those found in earlier single-crystal work. The former distance was calculated to be 22.5 Å while the latter data range from 22.1 to 22.7 Å.[78]

(82) For extended solids: *C*/2*m*, 163 compounds; *Cmn*, 13 compounds; *C*2, 15 compounds. See: Villars, P.; Calvart, L. D. *Pearson's Handbook of Crystallographic Data for Intermetallic Phases*, 2nd ed.; ASM International: Materails Park, 1991.

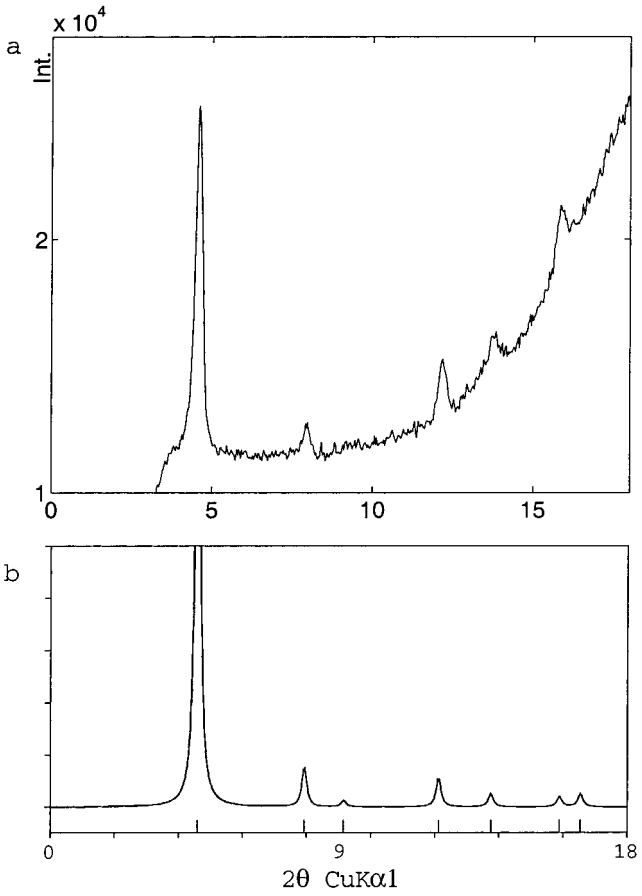

Figure 7. (a) Observed and (b) calculated X-ray diffraction patterns for **4**·AgOTf.

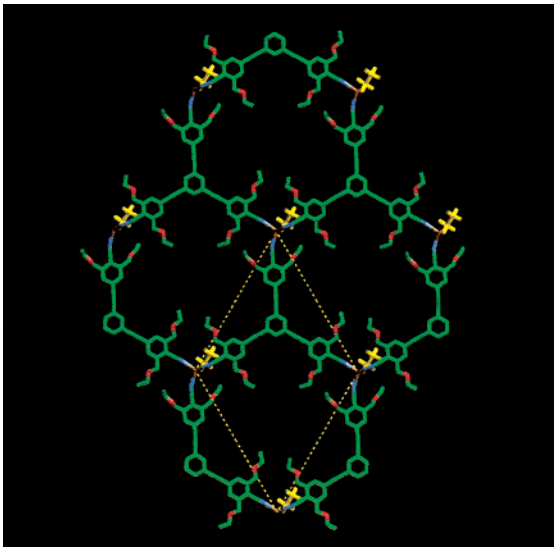

Figure 8. View down the channel direction of the model for **4**·AgOTf. The calculated diffraction pattern in Figure 7b is obtained from this model. Carbon atoms are shown in green, nitrogen in blue, oxygen in red, silver in brown, and triflate ions in yellow.

We have previously studied by X-ray methods a phenylacetylene nitrile·AgOTf single crystal whose molecular composition is the same as that of **4**·AgOTf except that the alcohol group of **4** is replaced by a methoxy group.[78] We therefore used this single-crystal structure to prepare a model for **4**·AgOTf. This structure was modified by removing the capping methoxy groups and then superimposing the remaining structure onto the refined hexagonally shaped cell. This model is shown in Figure 8. Due

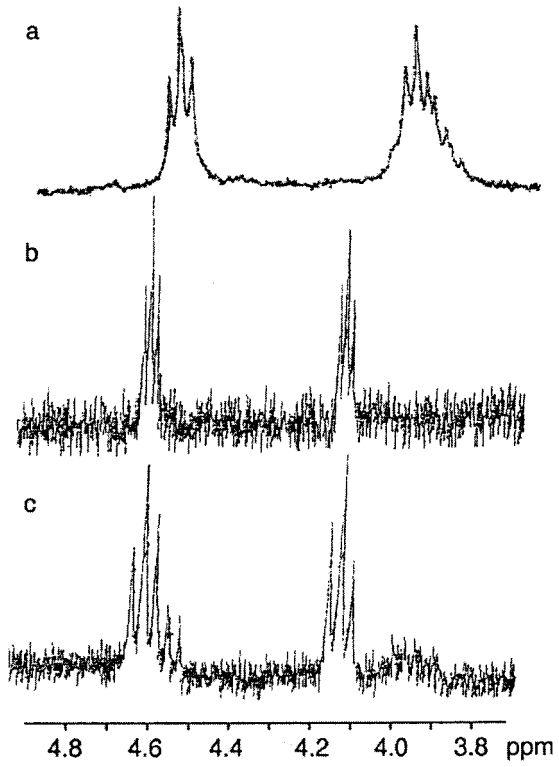

Figure 9. Portion of the 200 MHz ^{1}H NMR spectra in acetone-d_6 of (a) **3**, (b) **13**, and (c) **3** after solid-state reaction with *tert*-butyldimethylsilyl trifluoromethanesulfonate.

to the absence of symmetry in the side chains the model is oblique. The powder pattern based on this model is shown in Figure 7b. The agreement is fair. No refinement of any atomic parameters was made to improve the agreement between model and experiment. Furthermore, given that the side chains in **4**·AgOTf are probably involved in a hydrogen-bonded network and hence would adopt conformations different from those found in the methoxy derivative, the deviations found in Figure 7 appear understandable.

Solid-State Reaction of 3·AgOTf and *tert*-Butyldimethylsilyl Trifluoromethanesulfonate. As described in the Experimental Section, the solution reaction of molecule**3** and *tert*-butyldimethylsilyl trifluoromethanesulfonate occurs in quantitative yield at room temperature. The product is **13**. In Figure 9 we show the 4.0 to 5.0 ppm region of the ^{1}H NMR for both **3** and**13**. The peaks correspond to the side chain methylene group hydrogen atoms of these molecules.

By contrast the equivalent solid-state reaction between this same silyl monotriflate and **3**·AgOTf is slower and requires several days of **3**·AgOTf exposed to neat liquid *tert*-butyldimethylsilyl trifluoromethanesulfonate and 2,6-di-*tert*-butylpyridine, the neutralizing base used in the reaction. As described in the Experimental Section, after this time the solid-state portion is dried, the reaction mixture is quenched, and the resultant solid is dissolved in deuterated acetone. The ^{1}H NMR in the 4.0−5.0 ppm region of this dissolved material is shown in Figure 9. While the major compound found in Figure 9 is the silyl ether **13**, some unreacted **3** is also present based on the ^{1}H NMR data. The ratio of product to starting material is 4.5:1. Neither prolonged reaction time (up to three weeks) nor the addition of additional *tert*-butyldimethylsilyl trifluoromethanesulfonate to the reaction changes this ratio. Presumably in the solid state, there are alcohol sites which become inaccessible to attack by the guest silyl monotriflate.

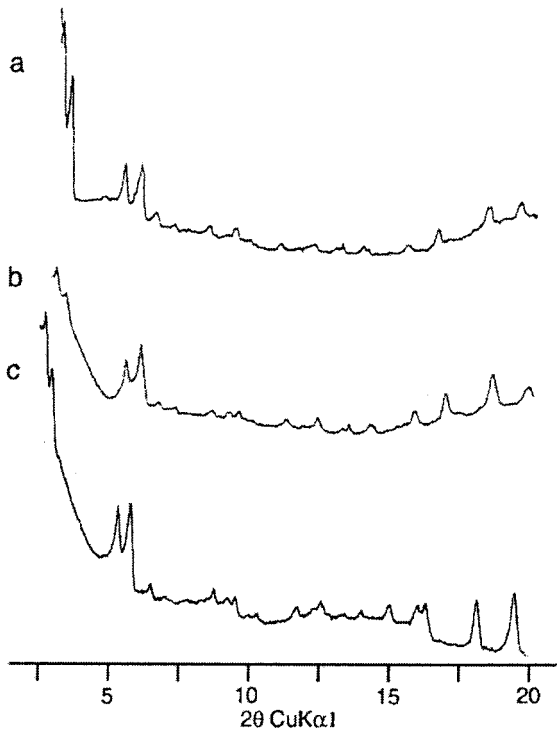

Figure 10. X-ray diffraction patterns for (a) **3**·AgOTf, (b) **13**·AgOTf, and (c) **3**·AgOTf after solid-state reaction with *tert*-butyldimethylsilyl trifluoromethanesulfonate. Patterns shown above are densitometer traces obtained from Guinier camera film.

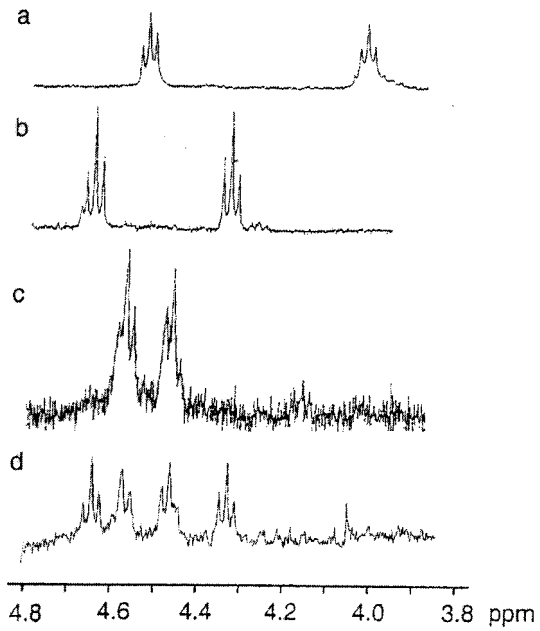

Figure 11. Portion of the 300 MHz ^{1}H NMR spectra in acetone-d_6 of (a) **3**, (b) **15**, (c) **14**, and (d) **3** after solid-state reaction with di-*tert*-butylsilyl bis(trifluoromethanesulfonate).

In Figure 10 we compare the Guinier camera powder pattern of the solid-state samples. Figure 10a gives the original X-ray pattern of unreacted **3**·AgOTf, Figure 10b corresponds to solution prepared molecule **13** subsequently crystallized with AgOTf, and Figure 10c shows the powder pattern of **3**·AgOTf after reaction with *tert*-butyldimethylsilyl trifluoromethanesulfonate. It may be seen that the three powder patterns shown here have the same general appearance. These results demonstrate that the solid-state portion retains the same crystal structure type during the **3**·AgOTf and silyl monotriflate reaction. Least-

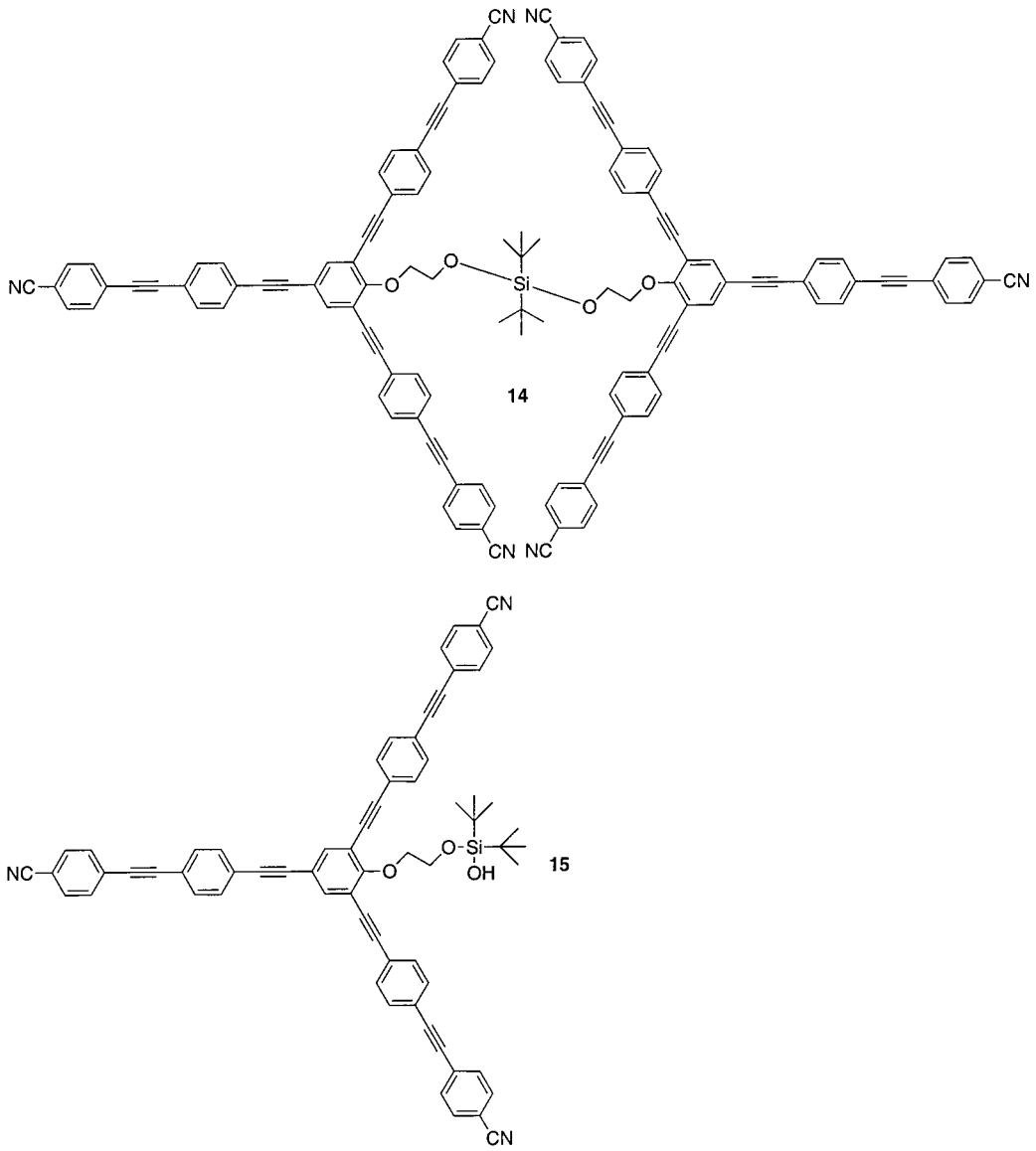

Figure 12. Organic molecules **14** and **15**.

squares refinement of these data shows though some variation in cell axis lengths. Between the three patterns, the *a* and *b* axes vary by respectively 1.0 and 0.5 Å, values 15 to 20 times greater than the standard deviations. These least-squares refinements are given in the Supporting Information.

The question remains as to whether the solid-state reaction truly occurs in the solid sate or whether some portion of the solid-state sample dissolves into solution, reacts with the silyl monotriflate in solution, and then recrystallizes into the honeycomb structure. The following point against this latter possibility. The reaction itself takes place in a minimum of liquid. No extra solvent is present, only the reactants themselves. Care was also taken to prevent reaction during the quenching of the excess silyl monotriflate. The quenching solvents, water and ethanol, were chosen as **3**·AgOTf is quite insoluble in these media, the solid product was subsequently dried under vacuum to pre-remove as much silyl monotriflate as possible, and finally ethanol and water are highly reactive with silyl monotriflate and thus during quenching there is little time for a reaction between **3** and silyl monotriflate to occur.

In this light, it is also of interest that we attempted the same solid-state silylation reaction with **2** (see Figure 1), a smaller phenylacetylene nitrile ligand with only four aromatic rings instead of the seven found in **3**. As reported earlier,[26] **2**·AgOTf also crystallizes in a honeycomb structure. While the solution reaction of **2** and *tert*-butyldimethylsilyl trifluoromethanesulfonate is facile and occurs in quantitative yield to form compound **12**, by ^{1}H NMR the solid-state reaction mixture of **2**·AgOTf and *tert*-butyldimethylsilyl trifluoromethanesulfonate shows no sign of reaction after 5 days. Furthermore, as is expected for a smaller molecule, **2** is generally more soluble than **3**. Were the previous reaction of **3**·AgOTf and *tert*-butyldimethylsilyl trifluoromethanesulfonate to have occurred by a dissolution, reaction, and subsequent recrystallization mechanism, it would be reasonable to expect that **2**·AgOTf would similarly react with the silyl monotriflate. That the reaction does not occur suggests a crystalline property of **2**·AgOTf is important. Recalling the initial sluggishness of the reaction between **3**·AgOTf and the silyl monotriflate, it is reasonable to suppose that in the more spatial constrained channels of **2**·AgOTf, reaction might not occur at all.

These results further exclude the possibility of the dissolution, reaction, and subsequent recrystallization mechanism.

Solid-State Dimerization of 3·AgOTf and Di-*tert*-butylsilyl Bis(trifluoromethanesulfonate). We now turn to the reaction of **3** and **3**·AgOTf with the silyl di-triflate molecule, di-*tert*-

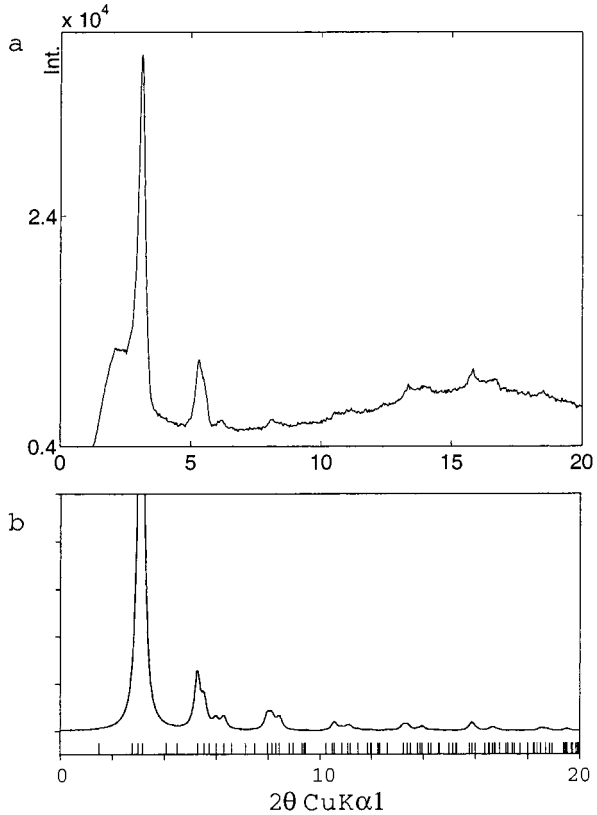

Figure 13. (a) Observed and (b) calculated X-ray diffraction patterns for **3**·AgOTf after solid-state reaction with di-*tert*-butylsilyl bis(trifluoromethanesulfonate).

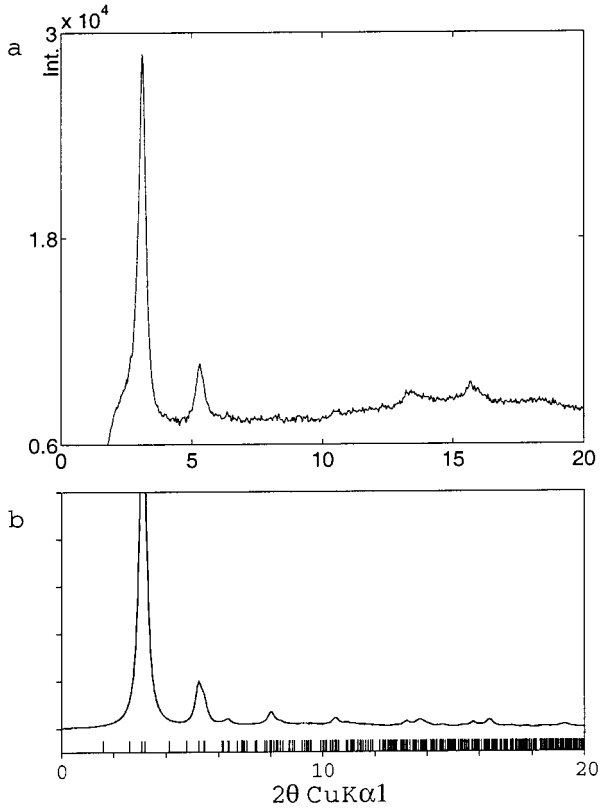

Figure 14. (a) Observed and (b) calculated X-ray diffraction patterns for **5**·AgOTf after solid-state reaction with di-*tert*-butylsilyl bis(trifluoromethanesulfonate).

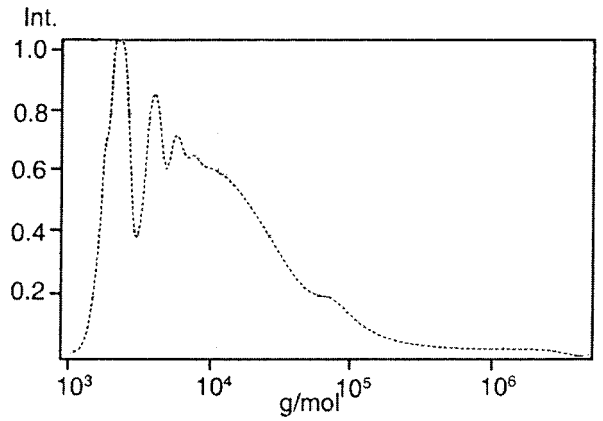

Figure 15. SEC trace for **5**·AgOTf after solid-state reaction with di-*tert*-butylsilyl bis(trifluoromethanesulfonate).

butylsilyl bis(trifluoromethanesulfonate). The reaction is substantially the same as in the previous example. However, the use of a di-triflate compound allows for two possible products, the monomer with a single Si−O linkage and the dimer with two **3** molecules linked to the same silicon atom. In Figure 11, we show the ^{1}H NMR signals for the hydrogen atoms of the methylene sites. Figure 11a,b shows the data for the solution-prepared monosubstituted and disubstituted compounds, respectively **14** and **15** (see Figure 12), while Figure 11c shows the pattern after the solid-state reaction of **3**·AgOTf with di-*tert*-butylsilyl bis(trifluoromethanesulfonate). The results indicate that the initial molecule **3**·AgOTf has completely reacted with an approximate 3:2 product ratio of dimer to monomer.

In Figure 13 we see the powder pattern of the solid-state portion of the reaction product. A comparison of Figures 3 and 13 shows that the overall crystal structure is maintained under these reaction conditions. Nevertheless, there are several substantial changes. In Figure 13 the major reflection s*110* and *200* are much closer in *d*-spacing. It is not possible to separate these two reflections from one another. The second pair of peaks, the *020* and *301* found near $2\theta = 5.3°$ are similarly fused. This change is reflected in the refined lattice constants. These lattice constants $a = 59.1(1)$ Å and $b = 31.95(7)$ Å are significantly different from those found for **3**·AgOTf. The *a* axis has increased by 7 Å, while the *b* axis has shortened by 2 Å. This *a* axis is reasonably close to the *a* axis of 59.5 Å found for the equivalently sized **5**·AgOTf. It also corresponds quite closely to the 60 Å length based on tabulated organic bond lengths. By contrast, in going from reactant to product, the *b* axis is shortened by 2 Å. These results suggest that vis-á-vis the two-dimensional projected crystal model, a rotation has occurred where the *a* axis is the axis of rotation. This same rotation in a projected cell has been found in one of our previously studied single-crystal structures.[11]

These results indicate a bulk property of the material has changed during the reaction. The least-squares refinement data are given in the Supporting Information and a calculated powder pattern based on this refinement is also given in Figure 13. Another change observed in the powder pattern is peak broadening of the reflections. Were **3**·AgOTf and di-*tert*-butylsilyl bis(trifluoromethanesulfonate) to have reacted in the multistep process of dissolution, reaction in the solution phase, and recrystallization, we would expect reasonably sharp reflections. The broadening of the peaks is suggestive that the reaction is occurring in the solid state and as the conditions of the reaction are not those of crystal annealing, damage to the crystal and subsequent line broadening occurs.

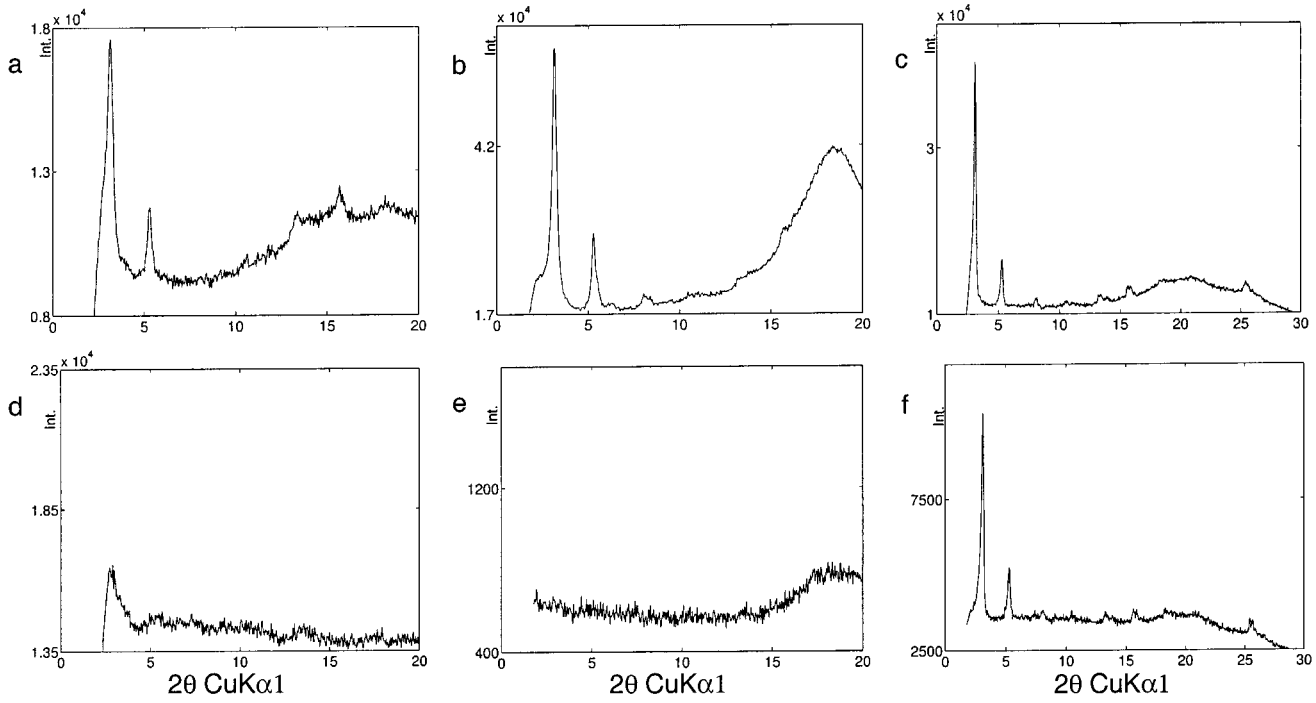

Figure 16. X-ray diffraction patterns for polymerized **5**·AgOTf immersed in (a) boiling water, (b) *t*-BuOH, and (c) acetone and for unpolymerized **5**·AgOTf immersed in (d) boiling water, (e) *t*-BuOH, and (f) acetone.

Solid-State Polymerization of 5·AgOTf and Di-*tert*-butylsilyl Bis(trifluoromethanesulfonate). This reaction was carried out under substantially the same conditions as in the previous two examples. However, a prolonged reaction time of three weeks was needed to drive the reaction to completion. Unlike the previous organic ligands, molecule **5** has three pendant alcohol groups. The number of possible products after reaction with the silyl ditriflate, di-*tert*-butylsilyl bis(trifluoromethanesulfonate), is therefore quite large, ranging from the monomer of **3**·AgOTf in which two of the three side chains have joined into one large macrocycle to oligomers and polymers of **5** with a statistical distribution of oxygen−silicon−oxygen linkages. The powder pattern of the reacted product is shown in Figure 14a. In comparing Figures 5 and 14a one sees significant changes in the crystal structure have occurred. While in Figure 5 there were two dozen identifiable reflections corresponding to a full three-dimensional cell, in Figure 14a no *hkl* ($l \neq 0$) reflections can be found below 25°. The *c* axis superstructure is therefore no longer observed. Even many of the *hk*0 reflections have broadened out and become indistinct. Besides the main *110* and *200* reflections only four additional peaks are found. The least-squares refinement in this refined data leads to an *a* axis of 57.3(3) Å and a *b* axis of 33.76(6) Å. The *a* lattice constant has changed by over 2 Å from the initial crystalline material, while the *b* axis is more or less constant.

An examination of the molecular weight of the reaction product is instructive. In Figure 15 we show size exclusion chromatography data of this product mixture. Monomer through tetramer peaks are clearly visible. These first four peaks are linearly spaced apart. The tetramer has an estimated molecular weight of 7×10^3, in reasonable agreement with what would be expected for a tetramer of molecule **5**, coupled through O−Si−O linkages and with all terminal hydroxy groups coupled to silyl di-*tert*-butyl groups (MW $5.5-6.0 \times 10^3$). Both fluorescence and refractive index measurements of sample mass are in fair agreement. The calculated average weight molecular weights M_w are respectively 6×10^4 and 7×10^4. Polydispersities are calculated to be 12 and 16.

As the data in Figure 15 are plotted on a log scale, there is considerably less monomer in the final product mixture than the peak profiles suggest. To verify that the quantity of monomer was low, we added to the product an additional amount of monomer equal in weight to half of the original product and then performed a size exclusion separation. These results are shown in the Supporting Information. From these data we can infer that the amount of monomer in the original reaction product is by weight just two or three percent of the total reaction product.

Finally, to verify that silver ions and silver−nitrogen bonds did not alter our weight distribution profiles we also performed a size exclusion separation on both pure **5** and **5**·AgOTf. These samples showed only the original monomer peak.

Exchange Properties of Polymerized 5·AgOTf. Our previous results indicate we have prepared microcrystalline materials in which the original **5** molecules in the crystal are now linked on the average to two of their neighbors. The interest in such a material is that by the inclusion of these covalent bonds we may have substantially improved the chemical stability of the crystalline material. We therefore exposed both the polymerized and original **5**·AgOTf to a variety of solvents which destroy related honeycomb structures. Solvents studied include acetone, *t*-BuOH, nitrobenzene, and boiling water. We also considered the thermal stability of the polymerized honeycomb structure, by heating a sample for a short time to 150 °C, a temperature just below the molecular decomposition temperature of **5**·AgOTf.

A few illustrative powder patterns are given in Figure 16. The remaining are given in the Supporting Information. As a comparison of Figures 14 and 16a−c shows, under these conditions, overall crystallinity is retained in the polymerized sample of **5**·AgOTf. By contrast as is seen in Figure 16d,e, both *t*-BuOH and boiling water turn unpolymerized **5**·AgOTf into

amorphous solids with practically no discernible diffraction peaks.

We further note that for the polymerized sample subjecting the material to boiling water or *t*-BuOH actually improves the overall crystallinity of the sample (compare Figures 14 and 16). These relatively strong conditions apparently allow for the annealing of the original polymerized crystals.

Finally in Figure 16c,f we show the powder patterns for both the original **5**·AgOTf and polymerized **5**·AgOTf after contact with acetone. For both samples, reasonably sharp powder patterns are observed. The first peak of the polymerized **5**·AgOTf has a full width half-maximum (fwhm) value of 0.15°. This fwhm value is fully the equal of any of the previously discussed powder patterns. We can find a lower estimate of particle size by assuming the entire line broadening is due to particle size. The classic Guinier formula[83] results in a minimum particle length of 530 Å. As there is substantial broadening due to both instrument factors and overlapping peak positions, particle size is expected to be significantly greater.

As a final characterization of porosity, we performed the vapor exchange experiments with toluene as described in the Experimental Section. An apohost (a host without included guest molecules) was prepared by heating the polymerized **5**·AgOTf in a Thermal Gravimetric Analysis (TGA) furnace to 150 °C for 10 min. This product was then exposed to two cycles of first being exposed to toluene vapor and subsequently being placed in a TGA furnace. The TGA data as well as the resultant powder data are given in the Supporting Information. These results indicate the polymerized material is still porous and absorbs 12−13 wt % of toluene molecules. The powder patterns of the final material show that the overall structure is retained, albeit with a significant reduction in the crystalline particle size.

(83) Guinier, A. *X-ray Diffraction in Crystals, Imperfect Crystals, and Amorphous Bodies*; Dover Publications: New York, 1994; p 143.

Acknowledgment. This work was supported by the National Science Foundation (Grant DMR-9812351). We thank Professors Geoffrey Coates and D. Venkataraman for advice and Dr. Ivan Gistov for assistance in obtaining the SEC results. We also thank Mr. Abhijit Basu Mallik for assistance in preparing compounds **8**−**11**.

Supporting Information Available: Tables and figures of X-ray powder diffraction data, tables of atomic coordinates for structure models of **3**-**5**·AgOTf, and SEC and TGA data (PDF). This material is avaliable free of charge via the Internet at http://pubs.acs.org.

JA0009119